

Article

# Revisit the Role of Steps/Disconnections on Misfit Cancellation at Semi-Coherent Interface—Bridging the O-Line Model and the Topological Model

Dong Qiu 

Centre of Additive Manufacturing, School of Engineering, RMIT University, Melbourne, VIC 3001, Australia; dong.qiu2@rmit.edu.au

Received: 15 September 2019; Accepted: 10 October 2019; Published: 13 October 2019



**Abstract:** It has been a long-standing topic how the lattice misfit is cancelled at a semi-coherent interphase boundary consisting of terraces and steps. Apart from a set of misfit dislocations separating the coherent patches, the role of steps (which is frequently called ‘disconnections’) on misfit cancellation remains ambiguous because these steps do not destroy the continuity of lattice planes across the interface. This paper aims to clarify such ambiguity through identification of a set of secondary dislocations through a rigorous constrained coincidence site lattice (CCSL)/constrained displacive shift complete lattice (CDSCL) analysis. A semi-coherent interface between body-centred cubic (BCC) Cr-rich precipitate and face-centred cubic (FCC) Cu-rich matrix that holds a near N-W orientation relationship (OR) is used as an example to demonstrate the procedure to determine the secondary dislocations that are coincident with steps along the interface. The current approach does not only redefine the disconnections in the topological model, but also extends the description of interface structure from the O-line model. As a result, the ‘discrepancy’ between these two popular crystallographic models can be completely eliminated when the interface is required to contain a pair of parallel close-packed directions.

**Keywords:** crystallography; interface; misfit dislocations; phase transformations

## 1. Introduction

The semi-coherent interphase boundary containing terraces and steps is a common type of interface between the secondary phase and its matrix in many metals and alloys [1]. This is because the atomically flat interface is, in many cases, associated with higher interface energy due to the lattice mismatch between a pair of parallel conjugated terrace planes. Introducing regular steps connecting adjacent terrace planes with a small tilt angle can effectively increase the density of a good matching site (GMS) to minimise the interface energy. There are quite a few crystallographic models that describe the preferred orientation relationship (OR) and the interface orientation (IO) with respect to the terrace planes [1]. These models can be basically classified into two schools. All the models in School 1 are geometric models that relates the parent and product phases by a homogeneous transformation strain and treat both lattices as rigid bodies. The typical School 1 models include the O-line model [2], the invariant line model [3] and the edge-to-edge matching model [4]. The step spacing and riser plane are themselves *not* variables when OR and IO are calculated; they are subject to the calculated IO with respect to the nearest terrace plane. In contrast, the School 2 model—represented by the topological model [5]—starts from a coherent terrace plane where both lattices are constrained and share the coherency strain along the terrace. The step characters, which are called *disconnection*, are predefined on a basis of commensurate dichromatic pattern (CDP). Such differences in the hypothesis and working procedure usually yield a different description of the preferred OR and IO given the

same alloy system [6]. The resultant debate between the two schools has lasted for two decades and is still ongoing. It appears a ubiquitous phenomenon that people used to solve the problems within the framework of their own school, as it is supposed to be superior than the others and vice versa. As a result, there is very limited frank and in-depth communication between these two schools. This paper aims to provide some insights into two representative models from each school, i.e., the O-line model and the topological model, and to demonstrate how these two models can be bridged by re-interpreting the role of disconnections.

## 2. Materials and Methods

The theoretical framework of the O-line model [7,8] and the topological model [5,6] have been well documented in literature. However, it is rather difficult for the general readers to directly compare these two models because of the different hypothesis, as mentioned above, and the numerous matrix algebra involved in both models. This paper will provide a case study in a step-by-step style with plain math so that each variable involved can be clearly and correctly quantified by general readers.

The FCC/BCC transformation in a dilute Cu-Cr alloy is a classical system for crystallographic studies and a range of ORs between N-W and K-S OR have been reported [9–12]. In this paper, we choose a N-W OR with a  $(5\ 3\ 3)_f$  stepped interface between FCC Cu matrix and BCC Cr precipitates as a case study. For simplicity, we use a 2D approach for both models where a pair of closed-packed directions  $(-1\ 1\ 0)_f/(-1\ 0\ 0)_b$  are strictly parallel to each other and lie in the interface. Subscripts, 'f' and 'b', refer to FCC and BCC lattice hereinafter. Then the problem turns out to be (1) what is the tilt angle,  $\phi$ , between the conjugated terrace planes  $(1\ 1\ 1)_f/(0\ 1\ 1)_b$ , and (2) what is the inclination angle,  $\theta$ , between the long-range strain-free interface and the terrace plane. The lattice constants used in the following calculations are  $a_f = 0.3615$  nm for Cu matrix, and  $a_b = 0.2853$  nm for Cr precipitates to be consistent with previous studies [13].

## 3. Results

Firstly, let us apply the topological model to solve this problem. The topological model starts with an ideal N-W OR where the terrace plane  $(1\ 1\ 1)_f$  is parallel to  $(0\ 1\ 1)_b$ . The natural dichromatic pattern (NDP) by intersecting the two lattices along the  $[-1\ 1\ 0]_f//[-1\ 0\ 0]_b$  directions (x axis) is shown in Figure 1a. The lattice translation vector magnitude along the y axis  $//[-1\ -1\ 2]_f//[0\ -1\ 1]_b$ ,  $a_{fy}$  and  $a_{by}$ , are  $|[-1\ -1\ 2]_f|/4$  and  $|[0\ -1\ 1]_b|/2$ , respectively, where the '|'| means the magnitude of a vector. The numerical values of  $a_{bf}$  and  $a_{by}$  are given in Table 1. In order to achieve a fully coherent terrace plane, a CDP is set up in Figure 1b where the BCC lattice expands, and the FCC lattice shrinks uniaxially along the horizontal direction (y axis). The magnitude of the commensurate translation vector,  $\langle a_y \rangle$ , is the average value of  $a_{fy}$  and  $a_{by}$ . The resultant coherency strain is defined as

$$\varepsilon_{yy} = \frac{a_{by} - a_{fy}}{\langle a_y \rangle} \quad (1)$$

**Table 1.** The numerical solutions of orientation relationship (OR) and interface orientation (IO) determined by the topological model.

$\varepsilon_{yy}$	$b_y$ (nm)	$b_z$ (nm)	$\langle h \rangle$ (nm)	$\theta$ (°)	$\phi$ (°)	$\theta_f$ (°)	$\theta_b$ (°)
-0.0928	0.0704	-0.0070	0.2052	15.56	0.5420	15.83	15.28

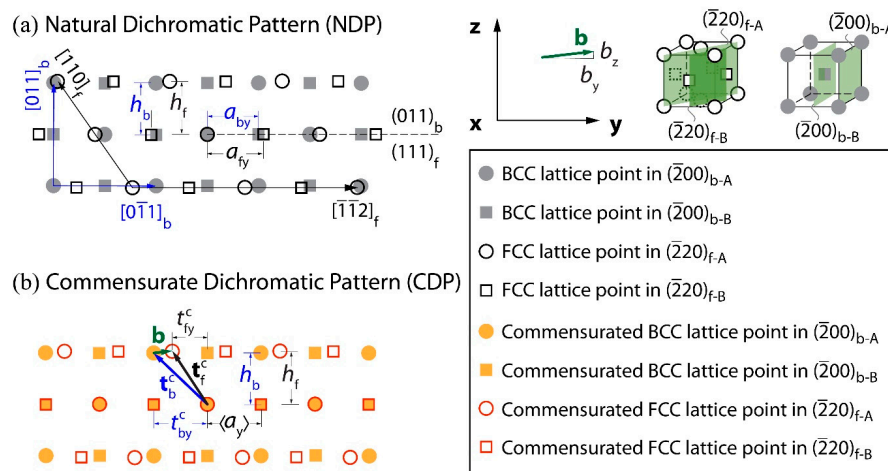


**Figure 1.** Identification of the variables of topological model at ideal N-W OR. (a) Natural dichromatic pattern; (b) Commensurate dichromatic pattern. Subscript ‘A’ and ‘B’ refers to the projection of alternating layers of  $(-2\ 0\ 0)_b$  and  $(-2\ 2\ 0)_f$ , both of which have an ABAB type stacking sequence. Axis  $x$  parallels  $[-1\ 1\ 0]_f // [-1\ 0\ 0]_b$ ; axis  $y$  parallels  $[-1\ -1\ 2]_f // [0\ -1\ 1]_b$ ; and axis  $z$  parallels  $[1\ 1\ 1]_f // [0\ 1\ 1]_b$ .

In the topological model, such a coherency strain is to be cancelled by introducing regularly spaced disconnections (or steps) between adjacent layers of terrace plane. The step vectors are denoted by  $t_f^c$  and  $t_b^c$  respectively. The superscript ‘c’ means the vector is defined in the CDP. The difference between  $t_f^c$  and  $t_b^c$  defines the displacement,  $b$ , as shown in Figure 1b. The horizontal and vertical components of  $b$  can be expressed by

$$b_y = t_{by}^c - t_{fy}^c \tag{2a}$$

and

$$b_z = h_b - h_f \tag{2b}$$

where  $t_{fy}^c$  and  $t_{by}^c$  are the horizontal components of  $t_f^c$  and  $t_b^c$ , while  $h_f$  and  $h_b$  are the step heights. The values of these components can be determined by

$$t_{fy}^c = |[-1\ -1\ 2]_f|/6 \cdot (1 + \epsilon_{yy}/2) \tag{3a}$$

$$t_{by}^c = |[0\ -1\ 1]_b|/2 \cdot (1 - \epsilon_{yy}/2) \tag{3b}$$

$$h_f = d_{(111)_f} \tag{3c}$$

and

$$h_b = d_{(011)_b} \tag{3d}$$

where  $d$  means interplanar spacing.

Supposing there is no long-range strain along the stepped interface, the component summation of  $b_y$ ,  $b_z$  and  $\epsilon_{yy}$  along the new interface should be zero. It should be noted that in the conventional topological model, the ‘overlap step height’ is employed to calculate the interface orientation [5,6]. However, it has been proved by the author that such a way is not mathematically rigorous [14]. A 2D reference lattice, rather than a CDP, must be set up when dealing with strain calculation on an inclined interface. The most intuitive 2D reference lattice is demonstrated in Figure 2. An average step height  $\langle h \rangle = (h_b + h_f)/2$  is used to replace the overlap step height,  $h$ , to maintain the rigour of strain calculation [14]. Then, the inclination angle  $\theta$  defined in the reference lattice can be calculated by solving the following equation [5,14]

$$b_z \tan^2 \theta + b_y \tan \theta + \epsilon_{yy} \langle h \rangle = 0 \tag{4}$$

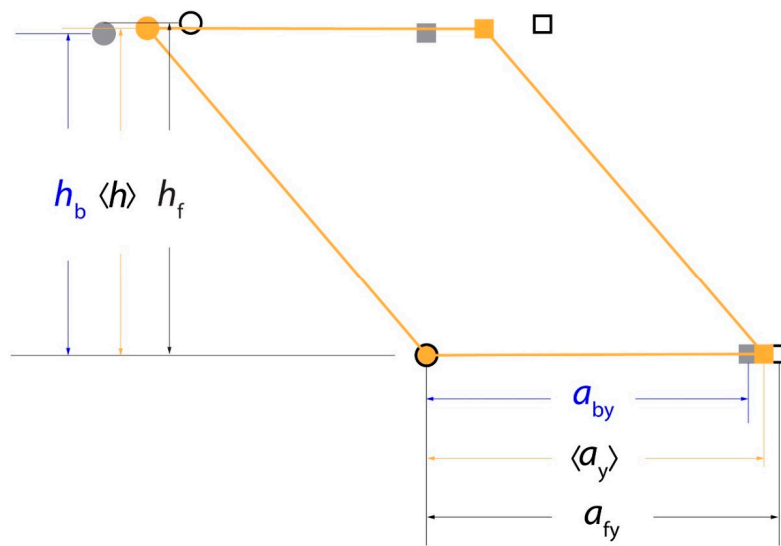


**Figure 2.** Definition of a 2D reference lattice (orange corners and orange edges) for strain calculation in an inclined interface. The circle and square patterns have the same meaning as those in Figure 1. Note the average step height  $\langle h \rangle$  rather than the overlap (i.e., smaller) step height is adopted to build this reference lattice.

Meanwhile the strain component normal to the stepped interface will be cancelled by a small tilt between the conjugated terrace planes  $(1\ 1\ 1)_f/(0\ 1\ 1)_b$ . The tilt angle  $\phi$  is given by [6,14]

$$\phi = 2 \tan^{-1} \left( \frac{b_z \tan}{2 \langle h \rangle} \right) \quad (5)$$

Considering the partitioning of the tilt angle into two lattices, the inclination angles of the stepped interface with respect to the terrace plane  $(1\ 1\ 1)_f$  and  $(0\ 1\ 1)_b$  can be expressed as

$$\theta_f = \theta + \phi/2 \quad (6a)$$

and

$$\theta_b = \theta - \phi/2 \quad (6b)$$

The numerical values of all above-mentioned variables in Equations (1)–(6) are summarized in Table 1. The stepped interface at this near N-W OR with all the disconnection characters is illustrated in Figure 3. Note that both lattices are plot in their natural form, rather than in the commensurate state. It can be seen that there is no lattice misfit at the centre of each terrace along the interface, witnessed by perfectly matched lattice points O and P separated by three disconnections. This indicates such an interface meets the long-range strain-free requirement.

Next, let us move onto the O-line model. Suppose the lattice misfit in the interface can be fully accommodated by a single set of misfit dislocations with the Burgers vector,  $[-1\ 1\ 0]_f/2 // [-1\ 0\ 0]_b$ , defined by the parallel closed-packed directions, then there is no lattice misfit component on the y-z plane in Figure 3. This means that the two lattices must be linked by a 2D invariant line strain defined in this y-z plane. The simplest way to describe such an invariant line strain is to apply the  $\Delta \mathbf{g}$  parallelism Rule II in the reciprocal space [8] through rotating the diffraction pattern of BCC lattice, relative to that of FCC lattice as explained below. Figure 4a shows the composite diffraction patterns along the zone axis parallel to  $[-1\ 1\ 0]_f/[-1\ 0\ 0]_b$ . The starting OR is an ideal N-W OR with  $(1\ 1\ 1)_f/(0\ 1\ 1)_b$  [DQ3]. The first  $\Delta \mathbf{g}$  is defined by

$$\Delta \mathbf{g}_{P-I-1} = \mathbf{g}_{(0\ 1\ 1)_b} - \mathbf{g}_{(1\ 1\ 1)_f} \quad (7a)$$

where  $\mathbf{g}_{(0\ 1\ 1)_b}$  and  $\mathbf{g}_{(1\ 1\ 1)_f}$  represent the reciprocal vectors associated with the terrace plane,  $(0\ 1\ 1)_b$  and  $(1\ 1\ 1)_f$ . Subscript 'P' means that it defines a principal O-lattice plane while subscript 'T' means the primary preferred state [1]. The second  $\Delta\mathbf{g}$  is defined by

$$\Delta\mathbf{g}_{P-I-2} = \mathbf{g}_{(0\ -1\ 1)_b} - \mathbf{g}_{(-1\ -1\ 1)_f} \tag{7b}$$

where the  $(-1\ -1\ 1)_f$  and  $(0\ -1\ 1)_b$  planes are another pair of closed-packed planes that contain the predefined Burgers vectors.

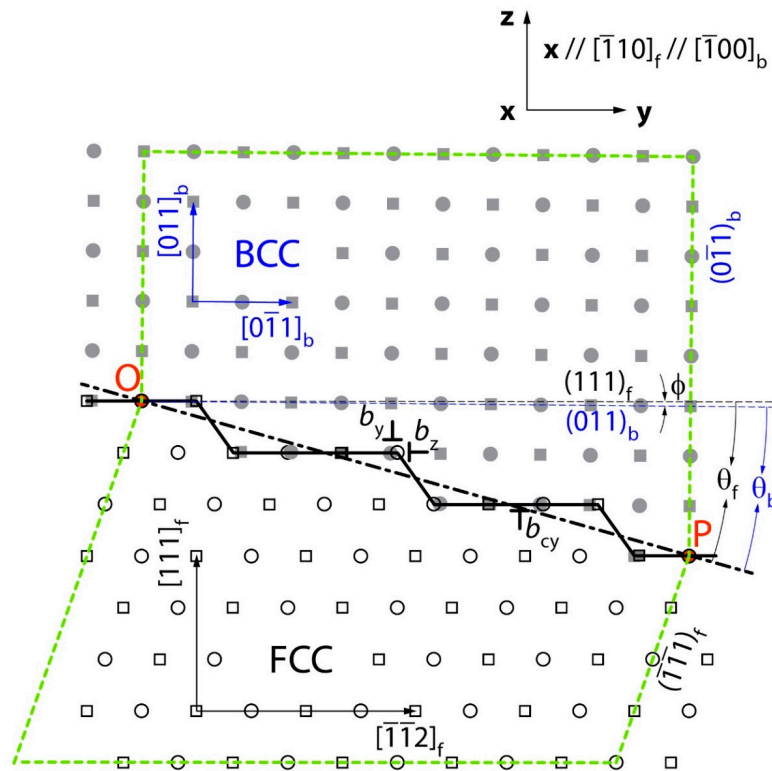


**Figure 3.** The topological version of the long-range strain-free interface containing a series of disconnections between FCC Cu and BCC Cr. The dashed-dotted line refers to the average orientation of the interface while the bold solid line outlines the actual interface consisting of terrace and steps. The green dashed lines indicate the Burgers circuit between perfectly matched lattice points O and P, located at terrace centres from different layers. The circle and square patterns have the same meaning as those in Figure 1.

As can be seen from Figure 4a, these two  $\Delta\mathbf{g}$ s are not parallel to each other at the initial N-W OR. A rigid body rotation about the common zone axes between two lattices is then needed to enable  $\Delta\mathbf{g}_{P-I-1}[\text{DQ4}] // \Delta\mathbf{g}_{P-I-2}$ . The rotation angle,  $\phi$ , can be expressed as [8]

$$\phi = \sin^{-1} \left( \frac{-s(1 + ab) \pm \sqrt{s^2 - (a^2 - 1)(b^2 - 1)}}{(a + b)^2 + s^2} \right) \tag{8}$$

where  $a = \frac{\sqrt{3}\lambda}{2}$ ,  $b = \frac{\sqrt{6}\lambda}{3}$ ,  $s = \frac{\sqrt{3}\lambda}{6}$  at a near N-W OR [8] and  $\lambda$  is the lattice constant ratio  $a_i/a_b$ . Figure 4b shows the composite diffraction patterns after this rotation is executed. Then, this pair of parallel  $\Delta\mathbf{g}$  vectors defines the normal of interface, and the angle between the interface and the terrace plane  $(1\ 1\ 1)_f$  is given by [8]

$$\theta_f = \sin^{-1} \left( \frac{2 + \sqrt{2}\lambda^2 \pm (4 + 3\sqrt{2})\sqrt{-2 + 3\lambda^2 - \lambda^4}}{2\sqrt{3}(3 + 2\sqrt{2})\lambda} \right) \tag{9}$$

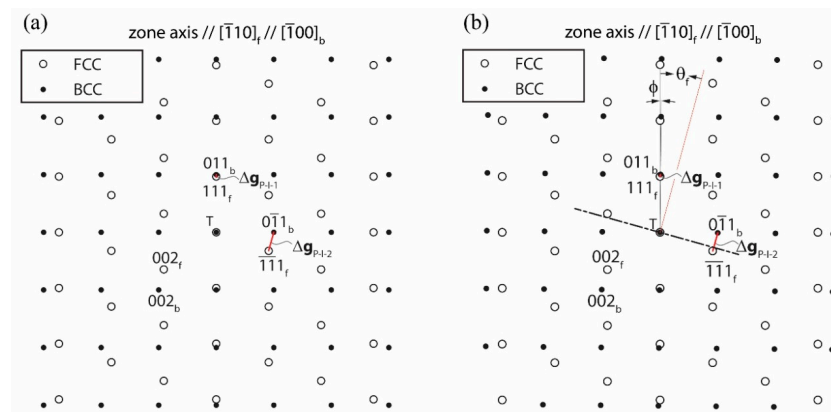


**Figure 4.** The 2D O-line approach to determine the OR and IO between FCC Cu and BCC Cr. (a) the composite diffraction patterns at ideal N-W OR. Two principal  $\Delta\mathbf{g}$  vectors are NOT parallel to each other; and (b) the composite diffraction patterns after the BCC lattice is rotated by  $\phi$  about the common zone axes. Two principal  $\Delta\mathbf{g}$  vectors are parallel to each other and define the average interface orientation (dashed-dotted lines).

The numerical values of rotation angle  $\phi$  and inclination angle  $\theta_f$  determined by the 2D O-line model is given in Table 2. Comparing the OR and IO determined by the topological model and the 2D O-line model, one can find that these two models give exactly the same results even though the working procedures are completely independent to each other. The same OR and IO determined by these two models in this case study is not a coincidence—because both models share the same constraint in essence, i.e., to maintain the local coherency on each terrace plane along the stepped interface. When the problem is restricted to 2D, there is only one degree of freedom between the two lattices, i.e., the tilt angle  $\phi$ , whilst the inclination angle  $\theta_f$  is dependent on  $\phi$ . This single degree of freedom can be fully fixed when the aforementioned constraint is applied. That explains why both models lead to the same OR and IO in this case study.

**Table 2.** The numerical solutions of OR and IO determined by the 2D O-line model.

$a$	$b$	$s$	$\phi$ (°)	$\theta_f$ (°)
1.0973	1.0346	−0.3658	0.5420	15.83

It seems that these two models can be easily harmonised based on the above analysis. However, it is worth mentioning that these two models have a distinctive description of the intrinsic line defects in the same inclined interface. In the O-line model, the consecutive steps along this interface are NOT associated with any lattice Burgers vectors. This can be easily validated in Figure 3. Drawing a Burgers circuit between the shared lattice points, O and P, separated by three steps, one can identify zero Burgers content because the circuit crosses 11 layers of  $(-1 -1 1)_f$  planes in the FCC lattice and also crosses 11 layers of  $(0 -1 1)_b$  planes in the BCC lattice. This sounds contradictory to the description given by the topological model where three disconnections are enclosed in this Burgers circuit. In the topological model, each disconnection is accompanied by a dislocation character with a ‘Burgers vector’,  $\mathbf{b}$ , as shown in Figure 1b. If this ‘Burgers vector’ is real, it should have been quantified by the Burgers circuit between O and P. This is a critical discrepancy that remains an unsolved issue between these two models and usually causes confusion for general readers.

As we can see from Figure 3, the misfit displacement around each disconnection is evident and it has opposite signs at the top and bottom of the disconnection. This is the typical character of misfit dislocation. If the Burgers vector of this misfit dislocation is not visualized from the Burgers circuit in Figure 3, there is only one possibility that this is a secondary misfit dislocation whose Burgers vector is not defined in either primary FCC or BCC lattice. In this section, a constrained CSL/DSCL

model is employed to quantify unambiguously this set of secondary misfit dislocations associated with each disconnection.

A constrained CSL (CCSL) in reciprocal space is constructed based on the initial N-W OR, as shown in Figure 5a. The BCC lattice is slightly distorted so that  $\mathbf{g}_{(0\ -3\ 3)_b}$  matches  $\mathbf{g}_{(-2\ -2\ 4)_f}$  while  $\mathbf{g}_{(0\ 1\ 1)_b}$  matches  $\mathbf{g}_{(1\ 1\ 1)_f}$ . Such a virtual distortion involves a compression of  $\mathbf{g}_{(0\ -3\ 3)_b}$  by 8.87% along the horizontal direction, and a compression of  $\mathbf{g}_{(0\ -1\ 1)_b}$  by 3.34% along the vertical direction. The resultant constrained DSCL (CDSCL) in direct space can be calculated according to the reciprocal relationship

$$\mathbf{G}_{\text{CCSL}}\mathbf{S}_{\text{CDSCL}} = \mathbf{I} \quad (10)$$

where  $\mathbf{G}$  and  $\mathbf{S}$  are 2D structural matrices defined in reciprocal and direct space, respectively. Given the basic vectors of 2D CCSL are  $\mathbf{g}_{(1\ 1\ 1)_f}$  and  $\mathbf{g}_{(-2\ -2\ 4)_f}$  in reciprocal space, the basic vectors of 2D CDSCL will be  $[1\ 1\ 1]_f/3$  and  $[-1\ -1\ 2]_f/12$  in direct space. They are denoted by  $\mathbf{b}_1^{\text{II}}$  and  $\mathbf{b}_2^{\text{II}}$  in Figure 5b respectively. The superscript 'II' represents the secondary preferred state. The basic vectors of this 2D CDSCL can also be expressed in the BCC lattice, i.e.,  $[0\ 1\ 1]_b/2$  and  $[0\ -1\ 1]_b/6$ . The Burgers vector of the secondary misfit dislocations is then shortlisted between  $\mathbf{b}_1^{\text{II}}$  and  $\mathbf{b}_2^{\text{II}}$ . Since the primary function of the secondary misfit dislocation is to cancel the misfit within the terrace plane, its Burgers vector should have a major component within the terrace plane. In this regard,  $\mathbf{b}_1^{\text{II}}$  is phased out because it is perpendicular to the terrace plane. Therefore, the only choice of the Burgers vector,  $\mathbf{b}^{\text{II}}$ , is  $\mathbf{b}_2^{\text{II}}$ , i.e.,  $[-1\ -1\ 2]_f/12$  or  $[0\ -1\ 1]_b/6$ .

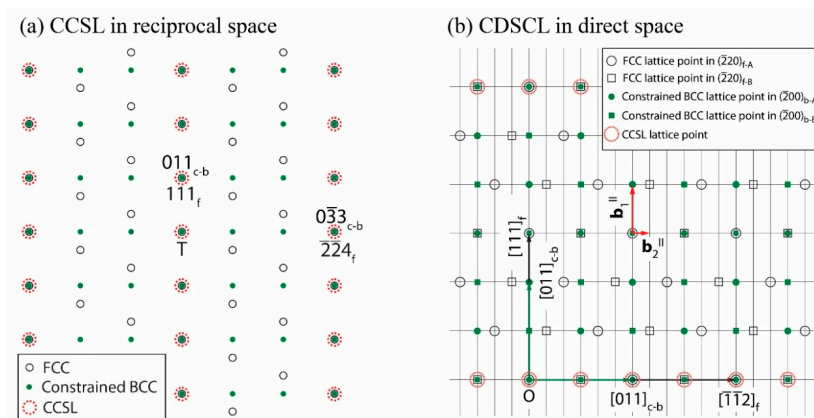


**Figure 5.** (a) The constructed CCSL in reciprocal space and (b) the correlated CDSCL in direct space at the ideal N-W OR. The two basic vectors of CDSCL are denoted by  $\mathbf{b}_1^{\text{II}}$  and  $\mathbf{b}_2^{\text{II}}$ . Note that the constrained BCC lattices are colored in green to distinguish themselves from those of natural BCC lattices.

The next step is to check whether the spacing of this set of dislocation is the same with the spacing of steps. The dislocation spacing can be calculated by the O-lattice model by using the characteristic triangles [1,15] in reciprocal space. Figure 6 shows how the characteristic triangles are identified on top of the composite diffraction patterns with Figure 4b. Firstly, for each characteristic triangle, one of its corners should lie on the trace of  $\mathbf{b}^{\text{II}*} = \mathbf{b}^{\text{II}}/|\mathbf{b}^{\text{II}}|^2$ . The superscript '\*' means it is defined in reciprocal space. Secondly, each characteristic triangle is enclosed by  $\Delta\mathbf{g}_{\text{II}}$ ,  $\mathbf{g}_{\text{terrace}}$  and  $\Delta\mathbf{g}_{//}$ , where  $\Delta\mathbf{g}_{\text{II}}$  is defined by a pair of CCSL vectors passing the trace of  $\mathbf{b}^{\text{II}*}$ ,  $\mathbf{g}_{\text{terrace}}$  is the reciprocal vector of the terrace plane, and  $\Delta\mathbf{g}_{//}$  parallels the interface normal,  $\mathbf{n}$ , defined by the principal CCSL vectors,  $\Delta\mathbf{g}_{\text{P-II}}$ . In this case study,  $\Delta\mathbf{g}_{\text{P-II}}$  is the same with  $\Delta\mathbf{g}_{\text{P-I-1}}$  in Figure 4b. Then the dislocation spacing can be expressed as

$$D_{\text{disl}} = |\mathbf{n}|/|\Delta\mathbf{g}_{\text{II}} \times \mathbf{n}| = |\Delta\mathbf{g}_{//}|/|\Delta\mathbf{g}_{\text{II}} \times \Delta\mathbf{g}_{//}| = 0.7653 \text{ nm} \quad (11a)$$

and the step spacing can be expressed as

$$D_{\text{step}} = |\mathbf{n}|/|\mathbf{g}_{\text{terrace}} \times \mathbf{n}| = |\Delta\mathbf{g}_f|/|\mathbf{g}_{\text{terrace}} \times \Delta\mathbf{g}_f| = 0.7653 \text{ nm} \tag{11b}$$

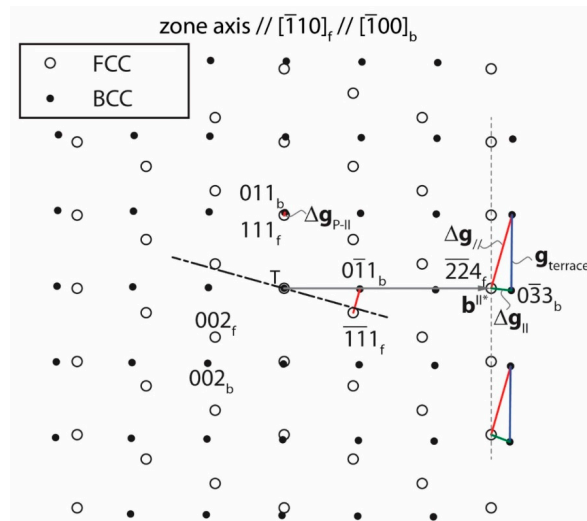


**Figure 6.** Identification of the characteristic triangles in reciprocal space based on the OR in Figure 4b. Note that all the red  $\Delta\mathbf{g}$  vectors are parallel to  $\Delta\mathbf{g}_{\text{P-II}}$  and normal to the interface.

The same spacing of secondary misfit dislocations and the interface steps guarantees that this set of secondary misfit dislocations are coincident with steps/disconnections along the interface, and accommodate the misfit within the terrace plane at each step/disconnection. Figure 7 shows the new Burgers circuits surrounding a step/disconnection based on the CDSCL in direct space. The constructed CDSCL is also overlaid on both sides of interface to help visualize the Burgers vector. Each Burgers circuit spans 10 layers of  $(-2 -2 4)_f$  and 11 layers of  $(0 -3 3)_b$  plane. Therefore, the Burgers vector,  $[-1 -1 2]_f/12$ , can be identified if the circuit is terminated in the FCC lattice and  $[0 -1 1]_b/6$  can be identified if the circuit is terminated in the BCC lattice. The results from this Burgers circuit analysis are fully consistent with what are derived from the CCSL/CDSCL analysis.

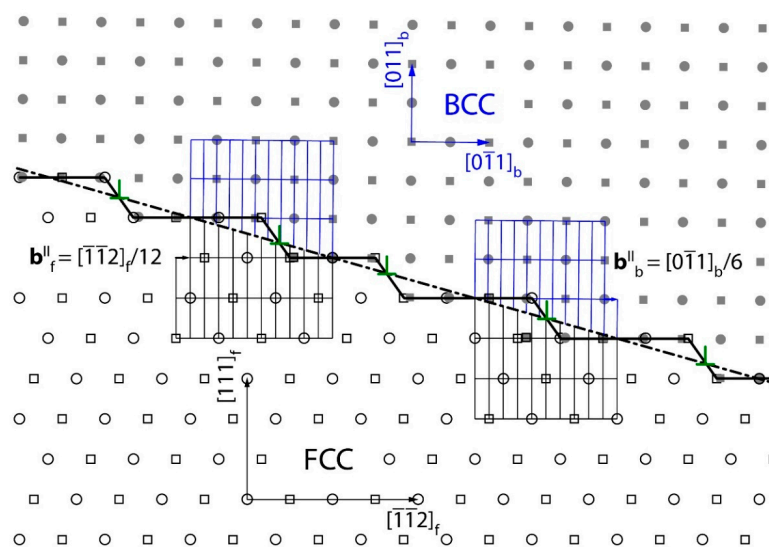


**Figure 7.** The secondary misfit dislocations ‘L’ at each step/disconnection. Two Burgers circuits are drawn in the CDSCL to identify the associated Burgers vectors expressed in the FCC and BCC lattices. The circle and square patterns have the same meaning as those in Figure 1.

## 4. Discussion

### 4.1. The Current Work vs. the Topological Model

The conventional topological model describes the Burgers vector at each step/disconnection by the misfit displacement,  $\mathbf{b}$ , defined in a CDP [5,6]. This description accompanies certain ambiguity since dichromatic pattern per se is NOT a lattice. It is well recognised that a Burgers vector is defined either as a shortest translation vector in parent/product lattice (primary misfit dislocations [15,16]) or as a shortest DSCL vector (secondary misfit dislocations [17]). In the current CCSL/CDSCL analysis, the Burgers vector is clearly defined as one of the basic vectors of the CDSCL so that such an ambiguity is completely avoided. The accurate description of the Burgers vector does not only help to clarify how the misfit at each step/disconnection is accommodated, but it is also critical to evaluate the elastic energy induced by this set of secondary misfit dislocations [5]. Then the contribution of steps/disconnections to the overall interface energy (at least its structural component) can be expressed as explicitly as the primary misfit dislocations in a semi-coherent interface. Note that the secondary misfit dislocations defined in the current study does not accommodate the small misfit component normal to the terrace plane, as illustrated by  $b_z$  in Figure 1b. Instead, this small misfit is accommodated through a small tilt,  $\phi$ , between a pair of terrace planes, as can be seen from Figure 3. Since the misfit normal to the terrace plane is usually much less than that within the terrace plane, i.e.,  $b_z \ll b_y$ , its contribution to the overall interface energy is negligible in most cases.

### 4.2. The Current Work vs. the O-Line Model

The current analysis also provides a supplementary description on top of a conventional O-line model. In the O-line model, the preferred interface is required to be a principal O-lattice plane containing periodic O-lines. For example, the vector  $\vec{OP}$  in Figure 3 defines an O-line in the y-z plane because there is no lattice misfit at any point lying in this line. Though the O-line model is mathematically rigorous, it can only describe the misfit accommodation in the mathematical interface (the dash-dotted line in Figures 3 and 7). When the principal O-lattice plane defined by the  $\Delta\mathbf{g}_{P-I-1} // \Delta\mathbf{g}_{P-I-2}$  is inclined to a pair of closed-packed planes, the interface must contain a series of terraces and steps. Whilst the centre of each terrace strictly lies in the principal O-lattice plane, the misfit that relates the lattice points close to the riser cannot be simply described by an invariant line strain. The current work manifests that these steps are not simply connecting the adjacent terrace planes along the inclined interface, but they also accommodate the misfit within the terrace plane through a set of secondary misfit dislocations. Such one-to-one correspondence between the interface steps and secondary misfit dislocations have been reported in many systems in a secondary preferred state, with a large difference of the lattice constants between the parent and product phases, for example, austenite/cementite [18],  $\text{Mg}_{17}\text{Al}_{12}/\text{Mg}$  [19] and  $\text{DySi}_2/\text{Si}$  [20]. However, the Cu/Cr case study used in this paper is a typical system in a primary preferred state with a definite one-to-one lattice correspondence between the FCC and BCC lattices. The CCSL/CDSCL model is, for the first time as far as the author knows, extended into the primary preferred state. The identified secondary misfit dislocations are compatible with the invariant line strain defined in a primary preferred state because the CCSL/CDSCL model is constructed based on the OR that enables the O-lines. As can be seen from Figures 4b and 6, the  $\Delta\mathbf{g}_{P-I-1}$  that defines the principal O-lattice plane in the primary preferred state also serves  $\Delta\mathbf{g}_{P-II}$  that defines the principal O-lattice plane in the secondary preferred state. As a result, both the Rule II and Rule III of the  $\Delta\mathbf{g}$  parallelism rules [1] can be applicable synergistically. It is expected that such a strategy can also be applied to describe the interface structure of the semi-coherent interface containing steps in other alloy systems when the CCSL/CDSCL is appropriately constructed.

It is worth pointing out that the crystallographic analysis in the current work is essentially a 2D version. In a 3D case where no parallel closed-packed directions exactly fall onto the interface, the OR and IO have one more degree of freedom compared to the 2D case. This means one needs an additional constraint to fix the OR and IO. Accordingly, the final solution will depend on the

selection of this constraint. Such an additional constraint can be either glissile misfit dislocations on the interface (which is equivalent to the Phenomenological Theory of Martensite Crystallography [21]), or maximum dislocation spacing on the interface (which is frequently used in the O-line model [7]), etc. The quantitative analysis of the role of disconnections/steps in a general 3D case is, hence, far more complicated than those in a 2D case, and it might be elaborated in a separate paper in the future.

## 5. Conclusions

- (1) The topological model can deliver the same OR and IO of a stepped, semi-coherent interface with those determined by a 2D approach of the O-line model when a 2D reference lattice is correctly defined. The discrepancy between the two models barely rests on the different description of the role of interface steps/disconnections.
- (2) The disconnections in the topological model can be explicitly described as regularly spaced interface steps coincident with a set of secondary misfit dislocations. The Burgers vector of the secondary dislocations,  $\mathbf{b}^{\text{II}}$ , is a partial lattice translation vector, defined by a basic vector of the CDSCL based on the OR that enables periodic O-lines.
- (3) In contrast to the primary misfit dislocations, which separate coherent patches in terrace planes, this set of secondary misfit dislocations do not destroy the continuity of lattice planes across the interface, and it only accommodates the extra misfit when the terrace plane is off the average interface, which cannot be described by the convention O-line model.
- (4) The one-to-one correspondence between the secondary misfit dislocations and the interface steps can be not only achieved in the secondary preferred state, but it can also appear in the primary preferred state when a 2D CDSL/CDSCL can be appropriately constructed.

**Author Contributions:** The main idea is proposed by the author and the full manuscript is written by the author.

**Funding:** This research received no external funding.

**Acknowledgments:** The author would like to thank Prof. Wenzheng Zhang who invited the author to contribute to this special issue.

**Conflicts of Interest:** The author declares no conflict of interest.

## References

1. Zhang, W.-Z.; Weatherly, G.C. On the crystallography of precipitation. *Prog. Mater. Sci.* **2005**, *50*, 181–292. [[CrossRef](#)]
2. Zhang, W.-Z.; Purdy, G.R. O-lattice analyses of interfacial misfit. II. Systems containing invariant lines. *Philos. Mag. A* **1993**, *68*, 291–303. [[CrossRef](#)]
3. Dahmen, U. Orientation relationships in precipitation systems. *Acta Metall.* **1982**, *30*, 63–73. [[CrossRef](#)]
4. Kelly, P.M.; Zhang, M.-X. Edge-to-edge matching—A new approach to the morphology and crystallography of precipitates. *Mater. Forum* **1999**, *23*, 41–62.
5. Howe, J.M.; Pond, R.C.; Hirth, J.P. The role of disconnections in phase transformations. *Prog. Mater. Sci.* **2009**, *54*, 792–838. [[CrossRef](#)]
6. Pond, R.C.; Celotto, S.; Hirth, J.P. A comparison of the phenomenological theory of martensitic transformations with a model based on interfacial defects. *Acta Mater.* **2003**, *51*, 5385–5398. [[CrossRef](#)]
7. Qiu, D.; Zhang, W.-Z. A systematic study of irrational precipitation crystallography in fcc/bcc systems with an analytical O-line method. *Philos. Mag.* **2003**, *83*, 3093–3116. [[CrossRef](#)]
8. Wu, J.; Zhang, W.-Z.; Gu, X.-F. A two-dimensional analytical approach for phase transformations involving an invariant line strain. *Acta Mater.* **2006**, *57*, 635–645. [[CrossRef](#)]
9. Hall, M.G.; Aaronson, H.I.; Kinsman, K.R. The structure of nearly coherent fcc: bcc boundaries in a Cu-Cr alloy. *Surf. Sci.* **1972**, *31*, 257–274. [[CrossRef](#)]
10. Hall, M.G.; Aaronson, H.I. The fine structure f.c.c./b.c.c. boundaries in a Cu-0.3% Cr alloy. *Acta Metall.* **1986**, *34*, 1409–1418. [[CrossRef](#)]

11. Fujii, T.; Nakazawa, H.; Kato, M.; Dahmen, U. Crystallography and morphology of nanosized Cr particles in a Cu-0.2% Cr alloy. *Acta Mater.* **2000**, *48*, 1033–1045. [[CrossRef](#)]
12. Luo, C.P.; Dahmen, U.; Westmacott, K.H. Morphology and crystallography of Cr precipitates in a Cu-0.33 wt% Cr alloy. *Acta Metall. Mater.* **1994**, *42*, 1923–1932. [[CrossRef](#)]
13. Qiu, D.; Shen, Y.-X.; Zhang, W.-Z. An extended invariant line analysis for fcc/bcc precipitation systems. *Acta Mater.* **2006**, *53*, 339–347. [[CrossRef](#)]
14. Kelly, P.M.; Qiu, D. The topological model (TM) of martensite transformations—Some improvements. *Solid State Phenomena* **2011**, *172–174*, 25–30. [[CrossRef](#)]
15. Zhang, W.-Z.; Purdy, G.R. TEM study of the crystallography and interphase boundary structure of precipitates in a Zr-2.5 wt% Nb Alloy. *Acta Metall. Mater.* **1993**, *41*, 543–551. [[CrossRef](#)]
16. Ye, F.; Zhang, W.-Z.; Qiu, D. A TEM study of the habit plane structure of intragranular proeutectoid precipitates in a Ti-7.26 wt% Cr alloy. *Acta Mater.* **2004**, *52*, 2449–2460. [[CrossRef](#)]
17. Howe, J.M.; Spanos, G. Atomic structure of the austenite-cementite interface of proeutectoid cementite plates. *Philos. Mag.* **1999**, *79*, 9–30. [[CrossRef](#)]
18. Ye, F.; Zhang, W.-Z. Coincidence structures of interfacial steps and secondary misfit dislocations in the habit plane between Widmanstätten cementite and austenite. *Acta Mater.* **2002**, *50*, 2761–2777. [[CrossRef](#)]
19. Zhang, M.; Zhang, W.-Z.; Ye, F. Interpretation of precipitation crystallography of Mg<sub>17</sub>Al<sub>12</sub> in a Mg-Al alloy in terms of singular interface structure. *Metall. Mater. Trans.* **2005**, *36A*, 1681–1688. [[CrossRef](#)]
20. Qiu, D.; Kelly, P.M.; Zhang, M.-X. The interfacial structure of self-assembled DySi<sub>2</sub> nanostructures grown on Si(0 0 1). *Scr. Mater.* **2009**, *60*, 787–790. [[CrossRef](#)]
21. Muddle, B.C.; Nie, J.F.; Hugo, G.R. Application of the theory of martensite crystallography to displacive phase transformations in substitutional nonferrous alloys. *Metall. Mater. Trans.* **1994**, *25A*, 1841–1856. [[CrossRef](#)]



© 2019 by the author. Licensee MDPI, Basel, Switzerland. This article is an open access article distributed under the terms and conditions of the Creative Commons Attribution (CC BY) license (<http://creativecommons.org/licenses/by/4.0/>).